Geometric quantum adiabatic methods for quantum chemistry

Hongye Yu (余泓烨),[1,2] Deyu Lu,[3,*] Qin Wu,[3] and Tzu-Chieh Wei[1,2,†]

[1]*C. N. Yang Institute for Theoretical Physics, State University of New York at Stony Brook, Stony Brook, New York 11794-3840, USA*
[2]*Department of Physics and Astronomy, State University of New York at Stony Brook, Stony Brook, New York 11794-3800, USA*
[3]*Center for Functional Nanomaterials, Brookhaven National Laboratory, Upton, New York 11973, USA*

(Received 30 December 2021; revised 16 June 2022; accepted 21 June 2022; published 15 July 2022)

Quantum algorithms have been successfully applied in quantum chemistry to obtain the ground-state energy of small molecules. Although accurate near the equilibrium geometry, the results can become unreliable when the chemical bonds are broken at large distances. For any adiabatic approach, this is usually caused by serious issues, such as energy gap closing or level crossing along the adiabatic evolution path. In this work, we propose a quantum algorithm based on adiabatic evolution to obtain molecular eigenstates and eigenenergies in quantum chemistry, which exploits a smooth geometric deformation by continuously varying bond lengths and bond angles. We demonstrate its utility in several examples on a noiseless quantum simulator, including H_2O, CH_2, and a chemical reaction of $H_2+D_2 \rightarrow 2HD$, by uniformly stretching chemical bonds. We find that this new algorithm solves the problems related to energy gap closing and level crossing along the adiabatic evolution path at large atomic distances. The new method performs more stably and achieves better accuracy than our previous adiabatic method [Yu and Wei, Phys. Rev. Research **3**, 013104 (2021)]. Furthermore, our fidelity analysis demonstrates that even with finite bond length changes, our algorithm still achieves high fidelity for the ground state.

DOI: 10.1103/PhysRevResearch.4.033045

I. INTRODUCTION

In recent years, quantum chemistry [1] has emerged as a promising domain science field where quantum computers can potentially lead to a breakthrough [2]. One important area is the ground-state total energy problem, where many systems exhibit strong character of many-body correlation effects (e.g., localized d and f electrons in transition-metal and rare-earth complexes), and a proper treatment is beyond the scope of widely used mean-field methods. As wave-function-based correlated methods remain computationally intractable against the system size on classical computers, various quantum algorithms, such as iterative quantum phase estimation (iQPE) [3], variational quantum eigensolver (VQE) [4,5], quantum adiabatic evolution (QAE) [6,7], and quantum annealing [8,9], have been proposed to tackle the ground-state total energy problem. Several quantum algorithms have been implemented and demonstrated for small molecules [2,4–6,9–12]. Further improved methods, such as the equation of motion [13] and the adaptive VQE [14], have also been designed. Some of us have previously proposed an adiabatic method that uses a particular interpolation from the maximally commuting (MC) Hamiltonian to the targeted full many-body molecular Hamiltonian [15]. Such a quantum adiabatic evolution from the initial MC Hamiltonian (MC-QAE) approach performs well for molecules near their equilibrium geometry, but the results become inaccurate at large atomic separations, due to energy crossing and the presence of dense low-lying energy levels. Previously we proposed a quantum Zeno approach to overcome this issue, which uses projection to instantaneous eigenstates of the discretized time-dependent Hamiltonian [15]. However, at present the spectral projection in the quantum Zeno approach requires QPE-like circuits and is less practical to implement than discretized Trotter evolution of the adiabatic Hamiltonian.

Here, we propose an adiabatic evolution method to compute ground-state and low-lying excited state energies of the many-body Hamiltonian of molecular systems along an adiabatic geometric path, which we refer to as the geometric quantum adiabatic evolution (GeoQAE). The GeoQAE starts with an initial geometry where MC-QAE can solve the ground state and low-lying excited states accurately. Then the system evolves adiabatically following a smooth geometric deformation by, e.g., stretching or compressing bonds and/or increasing or decreasing bond angles. We show that the GeoQAE approach does not suffer from the energy level crossing issue in the MC-QAE approach at large atomic distances. We further demonstrate its utility by computing the energies of the ground state and low-lying excited states of exemplary molecular systems, including H_2O and CH_2, as well as the potential energy surface of the chemical reaction of $H_2+D_2 \rightarrow 2HD$.

In addition, we show that the MC Hamiltonian proposed in our earlier work [15] is equivalent to the diagonal part of the full configuration interaction (CI) Hamiltonian in the qubit representation. The MC Hamiltonian in fact is closely related to the Hartree-Fock approximation, because under the fermionic basis it consists of diagonal one-body terms and

*dlu@bnl.gov
†tzu-chieh.wei@stonybrook.edu

two-body Hartree and Fock terms. We show that the Hartree-Fock ground state is an eigenstate of the MC Hamiltonian and the Hartree-Fock ground-state energy is the corresponding eigenenergy.

The remainder of the paper is organized as follows. In Sec. II, we briefly review the setup in the molecular Hamiltonian and discuss our choice of the initial Hamiltonian in the adiabatic evolution. In Sec. III, we present the GeoQAE approach and describe its protocol. There, we also present the analysis of the energy gap in the new adiabatic Hamiltonian to justify the approach. In Sec. IV, we show the results on noiseless quantum simulators of the GeoQAE approach applied to two molecules, H_2O and CH_2, which are more accurate than the previous MC-QAE approach and the quantum Zeno approach [15]. In Sec. V, we present a study on an idealized chemical reaction of $H_2+D_2 \rightarrow 2HD$, by computing the ground-state potential energy surface. In Sec. VI, we discuss the errors and fidelity from the perspectives of the choice of the geometric path, the evolution time T and the discrete step number M in an evolution. We also discuss the effect of Trotterization on the adiabatic evolution and the influence of gate errors using a simple noise model. We make concluding remarks in Sec. VII.

II. MOLECULAR HAMILTONIAN AND THE CORRESPONDING MAXIMALLY COMMUTING HAMILTONIAN

In this study, we focus on finding the ground state and low-lying excited states of molecular systems. For a given set of spin orbitals, the many-body Hamiltonian can be written in the second quantized form,

$$H = H^{(1)} + H^{(2)} = \sum_{i,j} t_{ij} a_i^\dagger a_j + \frac{1}{2} \sum_{i,j,k,l} u_{ijkl} a_i^\dagger a_k^\dagger a_l a_j, \quad (1)$$

where a and $a^\dagger$ are annihilation and creation operators, and i, j, k, l label the spin orbitals. The one-body hopping terms, t_{ij}, and two-body interacting terms, u_{ijkl}, are given by the following expressions:

$$\begin{aligned} t_{ij} &= \langle i|H^{(1)}|j\rangle \\ &\equiv \int dx_1 \chi_i(x_1) \left(-\frac{\nabla_1^2}{2} + \sum_\alpha \frac{Z_I}{|r_{1I}|} \right) \chi_j(x_1), \\ u_{ijkl} &= [ij \mid kl] \\ &\equiv \iint dx_1 dx_2 \chi_i^*(x_1) \chi_j(x_1) \frac{1}{|r_{12}|} \chi_k^*(x_2) \chi_l(x_2), \end{aligned} \quad (2)$$

where $\chi_i(x_1)$ are single-particle spin wave functions of orbitals i. Note that $[ij|kl]$ is expressed in the so-called chemists' notation and the same quantity is denoted as $\langle ik|jl\rangle$ in the physicists' notation [1]. In quantum chemistry calculations, Eq. (2) is usually evaluated on local atomic orbitals, known as the atomic basis set. While large basis sets can in principle lead to better numerical convergence toward the complete basis set limit, they require more qubits to implement the quantum algorithm. In this work the Slater-type orbital (STO)-3G basis (see, e.g., Refs. [1,16]) is used as a compromise between accuracy and computational cost, while our main conclusion does not rely on the choice of the basis set.

The goal of this work is to find the eigenstates and eigenenergies of Hamiltonian H of molecules, i.e., $H|\psi_E\rangle = E|\psi_E\rangle$, in particular the ground state and its energy, as well as low-lying states. To solve the problem on quantum computers, the above fermionic Hamiltonian needs to be converted to one composed of qubits. Several popular methods, such as the Jordan-Wigner, parity, Bravyi-Kitaev, and superfast Bravyi-Kitaev transformations [17–19], have been proposed to transform the fermion operators into Pauli operators,

$$H^P = \sum_i h_i P_i, \quad (3)$$

where P_i's are n-qubit Pauli operators and h_i's are the corresponding coefficients. For the results presented below, we use the parity and Jordan-Wigner transformation methods (see Appendix A).

Initial Hamiltonian and initial state

Next we express H in Eq. (1) in a set of molecular orbitals, denoted by Greek letters α, β, γ, etc., which are the solution of the Hartree-Fock Hamiltonian (see Appendix B). The superscript F indicates that it is expressed in fermionic field operators. The resultant Hartree-Fock states are single Slater determinants in this molecular basis. We emphasize the molecular basis by adding the superscript MO to the hopping and interaction coefficients, respectively,

$$H^F_{\text{full}} = \sum_{\alpha,\beta} t^{\text{MO}}_{\alpha\beta} a_\alpha^\dagger a_\beta + \frac{1}{2} \sum_{\alpha,\beta,\gamma,\delta} u^{\text{MO}}_{\alpha\beta\gamma\delta} a_\alpha^\dagger a_\gamma^\dagger a_\delta a_\beta. \quad (4)$$

For convenience, we denote the qubit version of H^F_{full} as H^P_{full}, where the superscript P corresponds to Pauli operators.

In the MC-QAE approach, our choice of the initial Hamiltonian H_I^P is the diagonal part of H^P_{full}, which only consists of products of Z terms and identities.

$$H_I^P = \sum_{P_i \in \{Z,I\}^{\otimes n}} h_i P_i, \quad (5)$$

where P_i's are from Eq. (3). Below we show that eigenstates of H_I^P, which are all in the quantum computational basis, correspond to single Slater determinants in the fermionic picture. A Slater determinant in H^F_{full} is the simultaneous eigenvector of the corresponding number operators $a_\alpha^\dagger a_\alpha$ for all α. Meanwhile, standard transformation methods (e.g., Jordan-Wigner, parity, Bravyi-Kitaev, and superfast Bravyi-Kitaev) map $a_\alpha^\dagger a_\alpha$ into Pauli Z terms, and $a_\alpha^\dagger a_\beta$ non-Z terms for $\beta \neq \alpha$. As a result, the diagonal part of H^P_{full} is the summation of all possible combination of $a_\alpha^\dagger a_\alpha$, $a_\alpha^\dagger a_\beta^\dagger a_\beta a_\alpha$, and $a_\alpha^\dagger a_\beta^\dagger a_\alpha a_\beta$. Therefore, the fermionic version of the initial Hamiltonian is

$$\begin{aligned} H_I^F &= \sum_\alpha t^{\text{MO}}_{\alpha\alpha} a_\alpha^\dagger a_\alpha \\ &\quad + \frac{1}{2} \sum_{\alpha,\beta} \left(u^{\text{MO}}_{\alpha\alpha\beta\beta} a_\alpha^\dagger a_\beta^\dagger a_\beta a_\alpha - u^{\text{MO}}_{\alpha\beta\beta\alpha} a_\alpha^\dagger a_\beta^\dagger a_\alpha a_\beta \right). \end{aligned} \quad (6)$$

We remark that the Hartree-Fock ground-state wave function is an eigenstate of H_I^F with eigenenergy E_{HF}. This can

be easily verified by directly applying H_I^F to the Hartree-Fock ground state $|\psi_{\rm HF}\rangle = |1..10..0\rangle$ that fills up orbitals with lowest energies,

$$H_I^F\ |\psi_{\rm HF}\rangle = E_{\rm HF}|\psi_{\rm HF}\rangle, \tag{7}$$

and obtaining $E_{\rm HF}$ as the Hartree-Fock ground-state energy,

$$E_{\rm HF} = \sum_{\alpha\in{\rm occ}} \langle\alpha|H^{(1)}|\alpha\rangle + \frac{1}{2}\sum_{\alpha,\beta\in{\rm occ}} ([\alpha\alpha\mid\beta\beta] - [\alpha\beta\mid\beta\alpha]), \tag{8}$$

where $[\alpha\beta|\gamma\delta] = u^{\rm MO}_{\alpha\beta\gamma\delta}$ in Eq. (4). More details are shown in Appendix C.

We remark that the Hartree-Fock ground state is also an eigenstate of the so-called Fock operator (also known as the mean-field Hartree-Fock Hamiltonian) $\hat{f}$ in Eq. (B7), but with an eigenenergy $\tilde{E}$ different from $E_{\rm HF}$ [1], due to the double counting in the interaction energy (i.e., a factor of two difference in the second term),

$$\tilde{E} = \sum_{\alpha\in{\rm occ}} \langle\alpha|H^{(1)}|\alpha\rangle + \sum_{\alpha,\beta\in{\rm occ}} ([\alpha\alpha\mid\beta\beta] - [\alpha\beta\mid\beta\alpha]). \tag{9}$$

For the molecules examined in Ref. [15] and this work, their H_I^P is the same as the initial Hamiltonian constructed by finding the maximum commuting set of terms in $H^P_{\rm full}$. For convenience, we will simply refer H_I^P as the maximally commuting (MC) Hamiltonian. Prior results on molecular systems [15] show that near the equilibrium geometry, a linear adiabatic evolution starting from the Hartree-Fock initial state can successfully drive the system from H_I^P to $H^P_{\rm full}$,

$$H(t) = \Big(1 - \frac{t}{T}\Big)H_I^P + \frac{t}{T}H^P_{\rm full}. \tag{10}$$

We remark that, as we shall see below in the case of CH_2 molecule, the Hartree-Fock state does not always lead to the final ground state. However, one can choose low-lying Hartree-Fock excited states or their superposition as the initial states. Since the electron number is conserved during the evolution, it is possible to choose an appropriate initial state with desired electron number. In special cases where the direct evolution fails because the symmetry of the system is not fully accounted for, one may use a symmetrized initial state instead to overcome the problem (see Sec. IV B). For example, given a MC Hamiltonian with two degenerate ground states $|\psi_1'\rangle = |01\rangle$, $|\psi_2'\rangle = |10\rangle$, we can prepare the initial state according to the spin configuration, e.g., a singlet state or a triplet state, which can be initialized by a short-depth circuit. Due to the symmetry preserved by both initial and final Hamiltonians, final ground states with different spin configurations can be evaluated separately from the corresponding initial states.

III. GEOMETRIC QUANTUM ADIABATIC EVOLUTION METHOD

Despite its good performance near the equilibrium geometry of molecules, the MC-QAE approach fails when chemical bonds are broken at large distances, due to energy gap closing or level crossing along the adiabatic evolution path. To overcome this problem, we propose the GeoQAE method as described below.

The GeoQAE is defined on an adiabatic path, where the geometry of the system evolves continuously characterized by an effective coordinate, $\boldsymbol{r}$. In simple cases, $\boldsymbol{r}$ can be atomic distance or bond angle, but more generally $\boldsymbol{r}$ can be associated with complex structural changes, such as phonon modes or reaction coordinates. In the examples presented this study, we only considered $\boldsymbol{r}$ as a specific atomic distance of small molecules (e.g., O-H distance in a gas phase water molecule), and generalization of $\boldsymbol{r}$ to more complex geometric changes is straightforward.

Suppose we have computed the ground state of the qubit Hamiltonian $H^P_{\rm full}(\boldsymbol{r}_0)$ for a molecule at $\boldsymbol{r}_0$ near the equilibrium position using, e.g., MC-QAE. In order to obtain the ground state and energy of $H^P_{\rm full}(\boldsymbol{r}_f)$ at large interatomic distances, we construct a series of Hamiltonians along the geometric path, $H^P_{\rm full}(\boldsymbol{r}_1), H^P_{\rm full}(\boldsymbol{r}_2), \ldots, H^P_{\rm full}(\boldsymbol{r}_N = \boldsymbol{r}_f)$, so that the sequence $\boldsymbol{r}_0$, $\boldsymbol{r}_1$, ..., $\boldsymbol{r}_N$ represents a gradual change in the atomic positions. Then we let the system evolve piecewise according to their interpolation as follows:

$$\begin{aligned} H_0^{\rm MC}(t) &= \Big(1 - \frac{t}{T}\Big)H_I^P(\boldsymbol{r}_0) + \frac{t}{T}H^P_{\rm full}(\boldsymbol{r}_0), \\ H_1^{\rm Geo}(t) &= \Big(1 - \frac{t}{T}\Big)H^P_{\rm full}(\boldsymbol{r}_0) + \frac{t}{T}H^P_{\rm full}(\boldsymbol{r}_1), \\ &\vdots \\ H_N^{\rm Geo}(t) &= \Big(1 - \frac{t}{T}\Big)H^P_{\rm full}(\boldsymbol{r}_{N-1}) + \frac{t}{T}H^P_{\rm full}(\boldsymbol{r}_N). \end{aligned} \tag{11}$$

For each step, the evolution from $H^P_{\rm full}(\boldsymbol{r}_i)$ to $H^P_{\rm full}(\boldsymbol{r}_{i+1})$ is likely to succeed due to the continuity of the Hamiltonian $H^P_{\rm full}(\boldsymbol{r})$ with respect to $\boldsymbol{r}$.

A. GeoQAE protocol

Details of the GeoQAE protocol are summarized as follows.

(i) Choose an initial effective coordinate, $\boldsymbol{r}_0$, of a molecule to construct the Hamiltonian and transform the fermion operators to Pauli operators;

(ii) Choose the terms only consisting of products of Z terms and identities to construct the initial Hamiltonian $H_I^P(\boldsymbol{r}_0)$ and construct the initial state $|\psi(0)\rangle$ from appropriate computational states, e.g., the Hartree-Fock ground state;

(iii) Discretize the time steps by $t_k = \frac{k}{M}T$ and obtain a series of Hamiltonians $H_0^{\rm MC}(t_k)$ in Eq. (11);

(iv) Perform the evolution operator $e^{-iH_0^{\rm MC}(t_k)\Delta T}$ on $|\psi(0)\rangle$ successively for $k = 1, \ldots, M$ and $\Delta T = T/M$, to reach one chosen eigenstate, which can be the ground state or a low-lying excited state, of the final Hamiltonian $H^P_{\rm full}(\boldsymbol{r}_0)$;

(v) Choose a suitable series of $\boldsymbol{r}$'s, $\boldsymbol{r}_1, \boldsymbol{r}_2, \ldots, \boldsymbol{r}_N$ with $\boldsymbol{r}_N$ being the target. Then repeat similar evolution procedure [steps (iii) and (iv)] for $H_i^{\rm Geo}(t)$, from the initial Hamiltonian $H^P_{\rm full}(\boldsymbol{r}_{i-1})$ to final Hamiltonian $H^P_{\rm full}(\boldsymbol{r}_i)$ consecutively with $N-1$ times.

We remark that steps (i)–(iv) are exactly the MC-QAE protocol, as GeoQAE uses MC-QAE as its first step at an appropriate $\boldsymbol{r}_0$. The total evolution time for getting the ground state of nth Hamiltonian $H^P_{\rm full}(\boldsymbol{r}_n)$ is nT. Below we denote $\tilde{T} \equiv nT$ as the accumulated evolution time. We normally

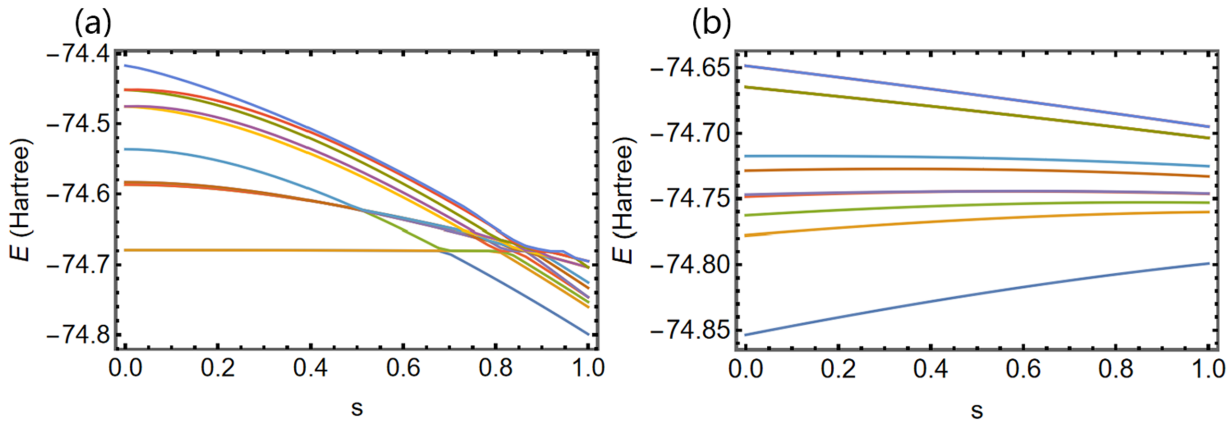

FIG. 1. Several lowest-energy levels of $H(s)$ for H_2O molecule at O-H distance $d = 1.758$ Å. In case (a), the evolution begins with maximum commuting Hamiltonian H_I^P at $d = 1.758$ Å [see Eq. (14)]; in case (b), the evolution begins the full Hamiltonian H_{full}^P at $d = 1.558$ Å and ends at the one at $d = 1.758$ Å [see Eq. (15)].

choose $\boldsymbol{r}_0$ near the equilibrium geometry, where the MC-QAE algorithm usually obtains the ground state accurately using, e.g., the Hartree-Fock ground state as $|\psi(0)\rangle$.

The performance of the GeoQAE can be measured by the error in the final ground-state energy. However, even if the energy is close, the final state $|\psi(\tilde{T})\rangle$ may not necessarily be close to the exact ground state $|\psi_g\rangle$. For this reason, we introduce the fidelity as an additional measure of the error in the eigenstate wave function [20]. We define the fidelity between two states $|\psi_A\rangle$ and $|\psi_B\rangle$ as

$$f(\psi_A, \psi_B) \equiv |\langle\psi_A|\psi_B\rangle)|, \tag{12}$$

and calculate $f(\psi_g, \psi(\tilde{T}))$ to see how close the final state $|\psi(\tilde{T})\rangle$ is to the ground state $|\psi_g\rangle$. In case of degeneracy where there are multiple $|\psi_{g,i}\rangle$'s with the same energy, then we will calculate the fidelity as follows:

$$f(\{\psi_{g,i}\}, \psi(\tilde{T})) = \sqrt{\sum_i |\langle\psi_{g,i}|\psi(\tilde{T})\rangle|^2}. \tag{13}$$

B. Energy gap analysis

To validate the GeoQAE method, we compare the energy spectrum of the MC-QAE path and GeoQAE path that both lead to the same final Hamiltonian $H_{\text{full}}^P(r_i = 1.758\ \text{Å})$ of the water molecule. The first one begins with the MC Hamiltonian $H_I^P(r_i = 1.758\ \text{Å})$ associated with the final Hamiltonian $H_{\text{full}}^P(r_i = 1.758\ \text{Å})$ at the same O-H distance,

$$H^{\text{MC}}(s) = (1-s)H_I^P(r_i) + sH_{\text{full}}^P(r_i). \tag{14}$$

The second Hamiltonian begins with the full Hamiltonian at a shorter O-H distance corresponding to an earlier position on the geometric path, $H_{\text{full}}^P(r_{i-1} = 1.558\ \text{Å})$ and ends with the final Hamiltonian $H_{\text{full}}^P(r_i = 1.758\ \text{Å})$,

$$H^{\text{Geo}}(s) = (1-s)H_{\text{full}}^P(r_{i-1}) + sH_{\text{full}}^P(r_i). \tag{15}$$

Their energy spectra as a function of s along two adiabatic paths are shown in Fig. 1. Clearly, there are multiple energy crossing points (e.g., near $s = 0.5$ and 0.7) in $H^{\text{MC}}(s)$, as shown in Fig. 1(a), and this is the reason that the direct MC-QAE fails. In contrast, $H^{\text{Geo}}(s)$ has energy levels smoothly connected without any crossing, as shown in Fig. 1(b). Thus, we see that the energy-crossing problem is solved by evolving from H_{full}^P of a nearby structure at $r_{i-1} = 1.558$ Å instead of the maximum commuting Hamiltonian at $r_i = 1.758$ Å. To obtain the ground state of $H_{\text{full}}^P(r_{i-1})$, one can construct $H^{\text{Geo}}(s)$ consecutively between r_{i-2} and r_{i-1}, r_{i-3}, and r_{i-2}, all the way to r_0 and r_1. In the end, as far as one can solve the ground state of $H_{\text{full}}^P(r_0)$ at r_0 using MC-QAE, the ground state of H_{full}^P along the adiabatic path from r_0 to r_i can be calculated accurately, eliminating the issue of energy level crossing.

IV. RESULTS ON MOLECULAR ENERGIES AND FIDELITIES

We apply the GeoQAE approach to three different systems H_2O, CH_2, and a chemical reaction $H_2 + D_2 \longrightarrow 2HD$. We numerically calculate the following evolution:

$$|\psi(T)\rangle \approx e^{-iH(T)\Delta T} e^{-iH(T-\Delta T)\Delta T} \ldots e^{-iH(\Delta T)\Delta T} |\psi(0)\rangle, \tag{16}$$

and evaluate the resultant energy on a noiseless quantum simulator, where $\Delta T = T/M$ and $|\psi(0)\rangle$ is a suitably chosen initial state. The molecular Hamiltonian (i.e., its coefficients t's and u's) is calculated with the PYSCF package [21] and transformed to Pauli operators with QISKIT [22]. The transformation we employ in this work includes the Jordan-Wigner transformation and the parity transformation. We also freeze the $1s$ orbital of C and O atoms. We use the Hartree-Fock state as our initial state, except for the case of CH_2, where a different initial state is required to obtain the correct H_{full}^P ground state (see details in Sec. IV B). We compare the GeoQAE results with the MC-QAE results that directly evolve from $H_I^P(r_i)$ to $H_{\text{full}}^P(r_i)$.

A. H_2O

Ground-state energy. For the gas phase H_2O molecule, we fix the H-O-H angle to be the equilibrium angle at $\theta = 104.45^\circ$ and compute the ground-state energy as a function of the O-H distance, d. The parity mapping method, along with

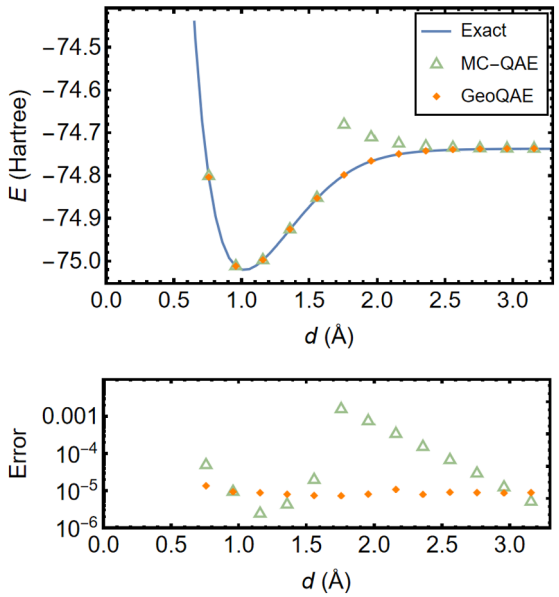

FIG. 2. Top: the ground-state energy of H_2O vs. the O-H distance, d, obtained with different approaches: classically exact diagonalization (solid curve), the MC-QAE (triangles), and the GeoQAE (dots). The H-O-H angle is fixed to the equilibrium angle $\theta = 104.45^\circ$. Bottom: relative errors in the ground-state energies using the MC-QAE and GeoQAE. $T = 40$ and $M = 20$ are used for both adiabatic methods. The GeoQAE may have larger errors when T and M are small, but the error can be reduced by increasing the two parameters.

the qubit reduction method and frozen O 1s orbital, are used to reduce and simplify the Hamiltonian to ten qubits.

In the GeoQAE calculation, we choose $r_0 = 0.958$ Å in the initial MC-QAE step with the Hartree-Fock state as the initial state to obtain the ground state of $H^P_{\text{full}}(r_0)$. Then we evolve H^P_{full} to $r_N = 3.158$ Å following the procedure outlined in Sec. III. Compared to MC-QAE, the GeoQAE method yields very accurate results with relative errors within 10^{-5} even at the very large atomic distances where MC-QAE fails, as shown in Fig. 2. Nevertheless, during the sequential evolution, the error will accumulate from all steps of evolution. Therefore, to achieve the same fixed accuracy at larger atomic distances, intuitively we may need more discretization steps M and a longer evolution time T. However, a recent study shows that the accumulating error in using Trotterization for the adiabatic evolution is not as severe as one would expect if the initial state is an eigenstate [23]. This is in line with what we have also observed in the bottom panel of Fig. 2 with $T = 40$ and $M = 20$ along the geometric path.

Ground-state fidelity. We also compute the fidelity of the final state of the adiabatic evolution $|\psi(\tilde{T})\rangle$ with the exact molecular ground state $|\psi_g\rangle$ of H^P_{full}. In these simulations we use evolution time $T = 40$ and discretize the continuous time evolution to $M = 20$ time slices. We compare the resultant ground-state fidelity between MC-QAE and GeoQAE. As we can see in Fig. 2, MC-QAE results agree with the exact solution near the equilibrium geometry and show a large error of 0.118 Hartree at $d = 1.758$ Å. This point can be seen clearly in Fig. 3, where the fidelity drops to zero beyond 1.758 Å.

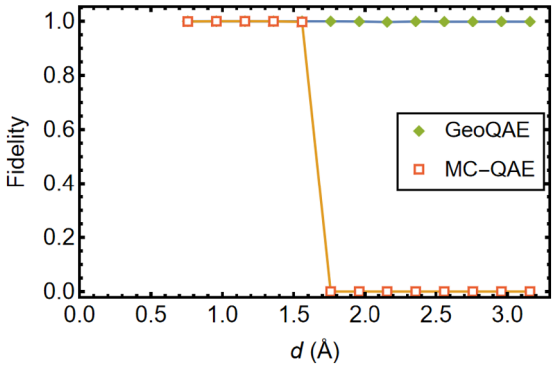

FIG. 3. The fidelity of the ground state of H_2O. The H-O-H angle is fixed to the equilibrium angle, $\theta = 104.45^\circ$. We set $T = 40$ and $M = 20$ for both methods.

The failure of the MC-QAE method can be understood, because the direct adiabatic evolution from H^P_I experiences level crossings and evolves into excited states at large d, which was reported in our previous work [15] and illustrated in Fig. 1(a). On the other hand, the final state evolved via GeoQAE does have the fidelity close to unity.

B. CH_2

CH_2 is an open-shell system and it presents a more challenging case for the GeoQAE method. Due to the facts that the ground state of CH_2 is a triplet state and the spin is conserved in both MC-QAE and GeoQAE methods, a triplet initial state has to be prepared in order to obtain the correct ground state.

Energy of the lowest few levels and the choice of initial states. For the CH_2 molecule, we fix the H-C-H angle to be the equilibrium angle at $\theta = 101.89^\circ$ and vary the C-H distance, d. Similar to the H_2O case, we freeze the 1s orbital of the C atom, and the number of spin orbitals and the number of electrons are reduced to 12 and 6, respectively. Since the lowest few states are not in the same spin configurations, we cannot use the qubit reduction method in parity transformation. We use the Jordan-Wigner transformation instead. In Fig. 4, we list the lowest six eigenstates of the MC Hamiltonian $H^F_I(r_0)$ from a closed-shell Hartree-Fock calculation in the occupation representation (spin up orbitals followed by spin down orbitals) at $r_0 = 1.109$ Å.

$$\phi_1 = |110000, 111100\rangle, E_1 = -10.540$$
$$\phi_2 = |111100, 110000\rangle, E_2 = E_1$$
$$\phi_3 = |110100, 110100\rangle, E_3 = -10.499$$
$$\phi_4 = |110100, 111000\rangle, E_4 = -10.487$$
$$\phi_5 = |111000, 110100\rangle, E_5 = E_4$$
$$\phi_6 = |111000, 111000\rangle, E_6 = -10.311,$$

where the energy is in Hartree units. The use of the frozen C 1s orbital leads to an extra energy shift (−33.895 Hartree) along with the nuclear repulsion energy of 6.034 Hartree. As shown in Fig. 4, in the eigenstates above, the first six binary numbers in the kets represent the occupation of the molecular orbitals with spin up (labeled as α) in the order of increasing energy and the last six numbers represent the occupation of

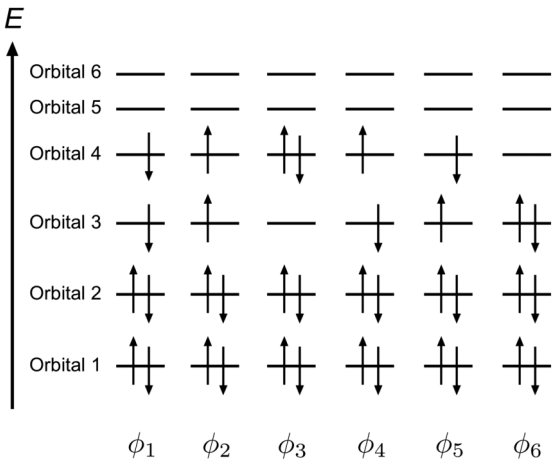

FIG. 4. The spin and orbital configurations for several lowest-energy states of $H_I^F(r_0)$ for CH_2 near its equilibrium position. The four orbitals are obtained from the Hartree-Fock procedure and the orbital 5 and 6 are empty for all the states we consider here.

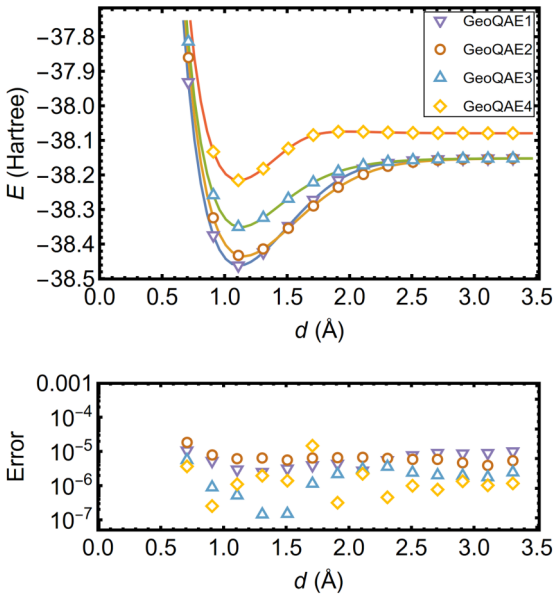

FIG. 5. The lowest four eigenstate energies of CH_2 versus the distance d between the C and H atoms with different initial states. The H-C-H angle is fixed to the equilibrium angle $\theta = 101.89°$. We choose $T = 60$ and $M = 30$ for all the cases. Top: The curves represent exact solutions from directly diagonalizing the Hamiltonian and the four different legends (labeled by GeoQAE1-4) represent results from simulated evolution on four different initial states (see the main text). The bottom panel displays the respective errors in targeting the eigenenergies.

the same set of molecular orbitals but with spin down (labeled as β).

ϕ_1 and ϕ_2 are degenerate triplet ground states. ϕ_4 and ϕ_5 are also degenerate, which differ by opposite spins in molecular spin orbitals 3 and 4 (see Fig. 4). The close-shell Hartree-Fock ground state turns out to be ϕ_6, which is the sixth excited state of H_I^P. Due to the fact that H_I^P and H_{full}^P conserve the total spin angular momentum and its z component, we can use linear combination of the degenerate single-Slater determinants to form the singlet and/or triplet states as the desired initial states. For example, from ϕ_4 and ϕ_5 we can construct a singlet $\psi_3 \equiv (\phi_4 - \phi_5)/\sqrt{2}$ and a triplet $\psi_{1,c} \equiv (\phi_4 + \phi_5)/\sqrt{2}$ initial states. For convenience, we also define $\psi_{1,a} \equiv \phi_1$, $\psi_{1,b} \equiv \phi_2$, $\psi_2 \equiv \phi_3$, and $\psi_4 \equiv \phi_6$.

By using these new sets of initial states, where $\psi_{1,a}$, $\psi_{1,b}$, and $\psi_{1,c}$ are triplet states, it turns out that ψ_1's under $H^{\text{MC}}(s)$ via the MC-QAE evolve into the triple degenerate ground states of the final Hamiltonian around the equilibrium position, while ψ_2, ψ_3, and ψ_4 separately evolve into three low excited states. We carry out the MC-QAE procedure numerically and verify that they indeed achieve the corresponding energies and eigenstates with over 99% fidelity. Subsequently, we proceed with the GeoQAE steps to obtain energies and wave functions at different d's that are both smaller and larger than r_0. As shown in Fig. 5, the three energy curves originating from ψ_1's, ψ_2, and ψ_3 remain the lowest, whereas the curve originating from ψ_4 evolves to an excited state at large molecular distances (as seen from its gap between the three lower curves). It is interesting that the lowest two energy curves cross, i.e., the threefold degenerate ground states become the first excited states at larger molecular distances. Given that these different levels have different symmetries, the adiabatic evolution will not mix them.

We remark that the superposition states, such as $\psi_{1,c}$ and ψ_3, are similar to the Greenberger-Horne-Zeilinger states and can be easily created and initialized by a short-depth circuit consisting of Hadamard and CNOT gates. In the above, ϕ_i's are calculated by direct diagonalizing the initial MC Hamiltonian, which is essentially classical (with Hamiltonian terms being products of Pauli Z and identity operators). Despite that finding the lowest configuration of a generic classical (e.g., Ising spin-glass) Hamiltonian can be NP, the time complexity of finding its low-lying states is still much less than those of the final quantum Hamiltonian for molecules. However, it is also not known whether the MC Hamiltonians from quantum chemistry problems are necessarily NP hard.

Fidelity with lowest three levels and the other excited level. In addition to the energy curves, we also calculate the fidelity of the evolved states $\psi(\tilde{T})$ with the corresponding numerically solved exact eigenstates ψ_E, and the results are shown in Fig. 6. Despite that the ground states (near equilibrium) are threefold degenerate, their spin configurations are different and hence their states can be numerically separated and distinguished, the use of the fidelity expression in Eq. (12) is appropriate.

From Fig. 6 we conclude that the GeoQAE can find all the lowest three levels and the other excited level (the latter corresponding to the fourth level around the equilibrium) with high fidelity. In contrast, the direct evolution from MC-QAE encounters serious problems at larger distances (not shown explicitly) [15], similar to the case of H_2O in the previous section.

V. CHEMICAL REACTION

The knowledge of the potential energy surface of a chemical reaction is critical to understand the reaction mechanism. In particular, reaction energies and reaction barrier heights

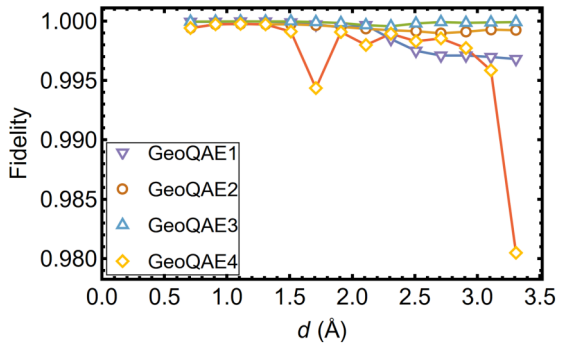

FIG. 6. The fidelity of CH_2 versus the distance d between the C and H atoms with different initial states. The H-C-H angle is fixed to the equilibrium angle $\theta = 101.89^\circ$. We choose $T = 60$ and $M = 30$ for all the cases.

(i.e., the energy differences between reactants/products and the transition state) are key quantities that dictate the reaction energetics. It is important to develop quantum algorithms to compute the reaction potential energy surface.

In the previous section, we have seen that molecular energies can be accurately obtained by the GeoQAE, which shows more robustness and wider applicability than the MC-QAE. As a further application, we now apply this method to explore the energy landscape of an exemplary chemical reaction: $H_2 + D_2 \longrightarrow 2HD$. In addition to a model system for proof of principle, such a system is also of interest in the context of experimental realization of cold controlled chemistry [24]. Below we do not consider the difference in the nuclear effects between H and D, which will influence the dynamics.

To reduce the complexity of the problem, we consider that the four atoms are initially set as the vertices of a rectangle with vertical edges from H_2 and D_2 (r_1) longer than horizontal edges from H. . .D (r_2), as shown in Fig. 7. We study the chemical reaction corresponding to simultaneously stretching r_2 while compressing r_1, such that H_2 and D_2 break apart and 2HD pairs are formed. In order to reveal the reaction pathway, it is crucial to obtain the accurate energy of the square configuration as the most important reaction intermediate [25]. We find that the MC-QAE method works fairly well for nonsquare configurations, but fails when the structure is close to a square, because of the energy crossing associated with the high symmetry of a square. For square configurations,

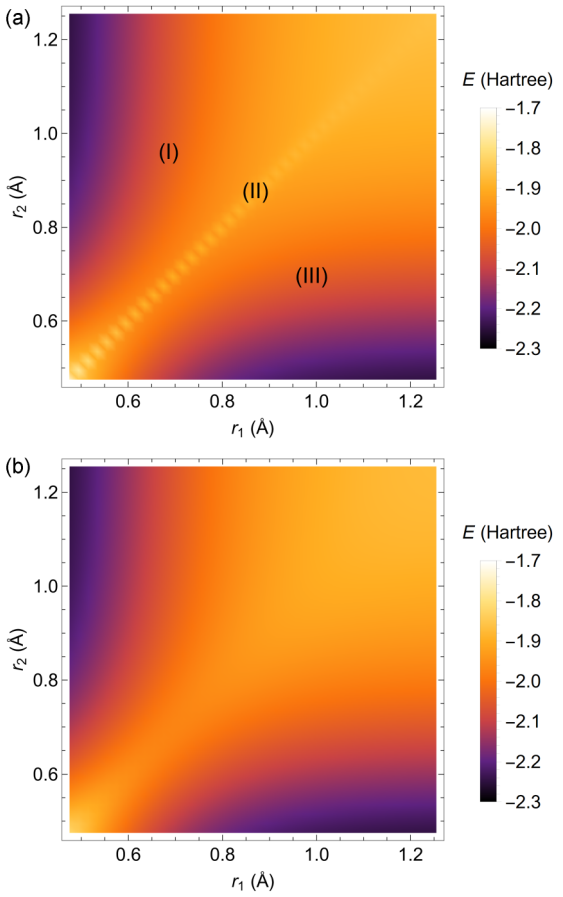

FIG. 8. (a) The results of the potential energy surface using MC-QAE. (b) The results of the potential energy surface after the correction from geometric adiabatic path. The distances r_1 and r_2 are in unit of Å. We choose $T = 80$ and $M = 40$ for both methods. The correction only takes place in the region between the two dashed lines in Fig. 9.

the GeoQAE performs more stable and accurate than the MC-QAE, as demonstrated in Figs. 8(a) and 8(b). In this study, we use the Jordan-Wigner mapping to convert the fermionic Hamiltonians to the corresponding qubit Hamiltonians with eight qubits. For the off-diagonal points representing unequal distances in Fig. 9, we use the MC-QAE for both cases. For the near-diagonal points, we use a two-step process: first we

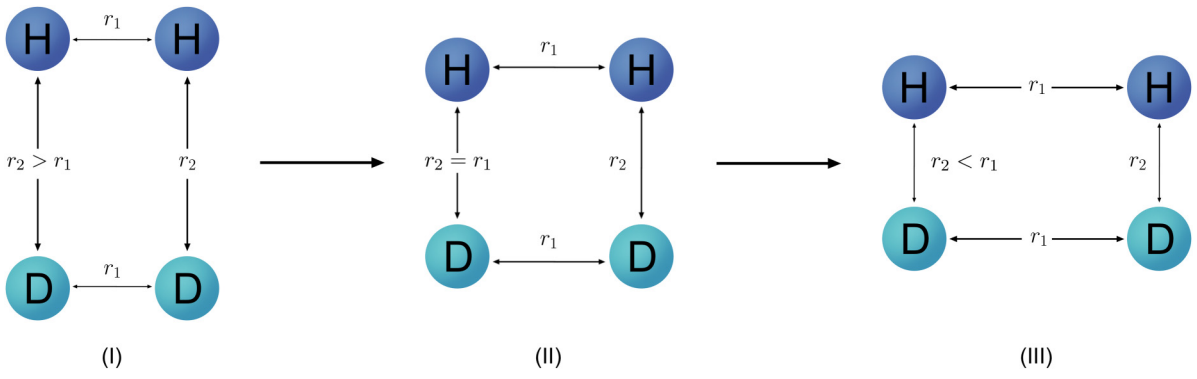

FIG. 7. The geometric configurations for chemical reaction H_2+$D_2 \longrightarrow 2HD$.

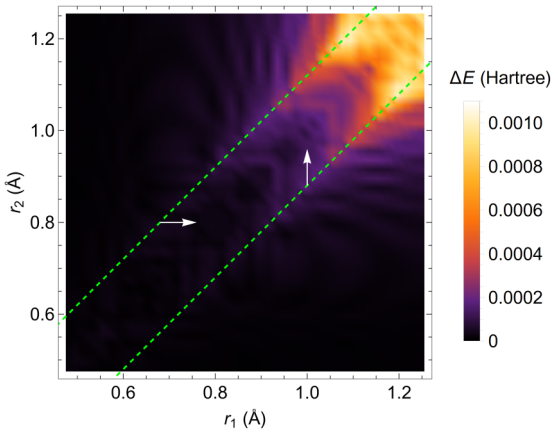

FIG. 9. The energy difference compared to the exact results of the potential energy. The points within the two dashed lines are calculated by GeoQAE evolving from the nearest (in the sense of keeping either r_1 or r_2 the same) boundary of this region. And the white two arrows show the two possible evolution directions. The points outside the dashed line is calculated directly from MC-QAE.

compute the ground state of the system at its nearest off-diagonal neighbor via the MC-QAE, then adiabatically evolve the system to its ground state at the diagonal point via the GeoQAE, which is illustrated by the arrows and green dashed lines in Fig. 9. For each run of evolution from one distance to another, we set $T = 80$ and $M = 40$.

The error in the ground-state energy between the GeoQAE and the exact solution is shown Fig. 9 and the results are very accurate except in the region of larger r's, which can be improved by using larger M and T (see, e.g., Sec VI). In Fig. 10, we explicitly compare the results of the MC-QAE and GeoQAE at $r_1 = r_2$, i.e., the square configuration. We find that the energies from the MC-QAE are substantially higher than those from the GeoQAE (e.g., by 3.6% at 1.390 Å), with the latter having 10^{-4} relative errors or smaller. This again underscores the remarkable advantage of the GeoQAE in regions where the MC-QAE fails.

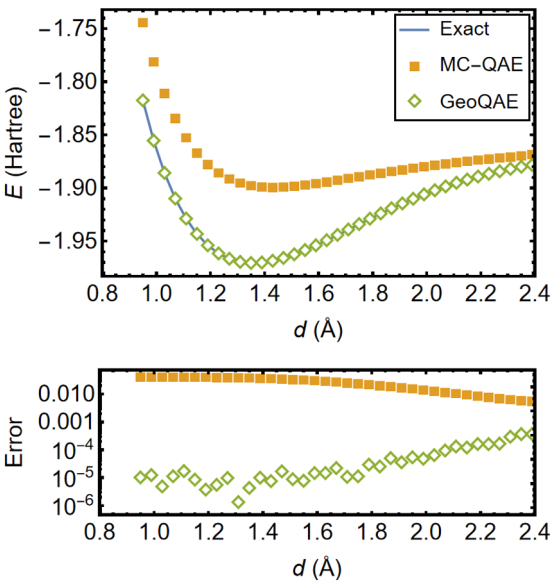

FIG. 10. Top: The results of the potential energy along the $r_1 = r_2 \equiv d$ line for two different methods, MC-QAE and GeoQAE. The bottom panel shows the relative errors from the two methods.

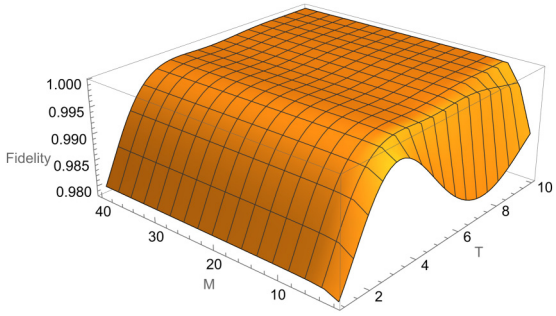

FIG. 11. The results of the fidelity vs. M and T using the H_2O molecule as an illustration. The evolution is from H_I^P to H_{full}^P at O-H distance $d = 0.958$ Å.

VI. ERROR ANALYSIS AND COMPUTATIONAL COMPLEXITY

Apart from the possible noise and error from real quantum computers discussed in our previous paper [15], the intrinsic error of the GeoQAE method mainly depends on three factors: the evolution time T, the discretizing step number M, and the discretization of geometric path. We discuss each of them below.

A. Effects of evolution time T and discretization number M

The evolution time T and discretization number M control the degree of adiabaticity and discretization rate, respectively. If a finite energy gap is maintained along the adiabatic evolution path, one can theoretically achieve arbitrarily high accuracy by choosing sufficiently large T and M. However, such large values are not necessarily practical, because large number of gates will lead to the accumulation of noisy gate errors. In our simulations, we usually choose T to be inversely proportional to the minimum gap of the evolution, and fixed the ratio of T/M to keep the discretization error small. However, one may not necessarily have the information on the gaps, and may need to empirically test a few choices to see if the energy reaches the convergence as T increases. We test the influence of T and M on the fidelity with the ground state and find that T has larger impact than M on the fidelity as shown in the Fig. 11. As one can see, while the fidelity along the M axis is almost constant, it exhibits a much larger variation along the T axis. For $M \geqslant 5$, the fidelity increases as a function of T from ∼0.98 and quickly plateaued close to 1.

B. Effects of Trotter decomposition

To simulate quantum evolution on current gate-based quantum computers, one needs to perform Trotter decomposition to reduce the evolution operator to simple Pauli rotations. For one-step evolution $e^{-iH\Delta t}$ of Hamiltonian $H = \sum_j h_j P_j$,

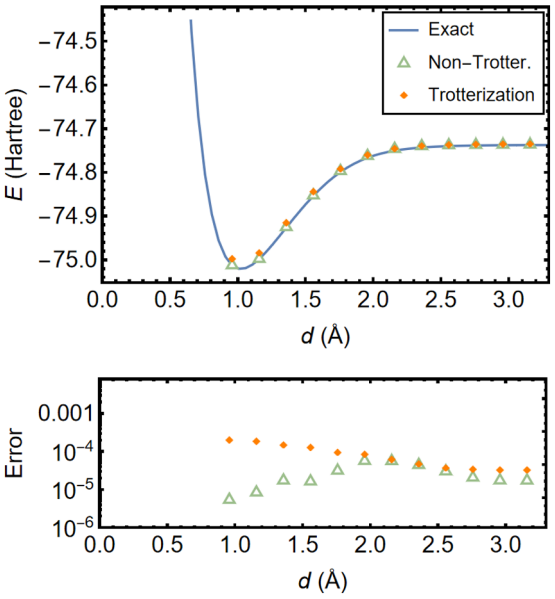

FIG. 12. Top: the ground-state energy of H_2O versus the O-H distance, d, obtained with different approaches: exact diagonalization (solid curve), the GeoQAE with exact discrete evolution operators (triangles), and the GeoQAE with Trotter expansions (dots). The H-O-H angle is fixed to the equilibrium angle $\theta = 104.45^\circ$. Bottom: relative errors in the ground-state energies using the MC-QAE and GeoQAE. $T = 10$ and $M = 20$ are used for both methods.

where P_j are Pauli operators, a naive first-order Trotter expansion is simply

$$e^{-iH\Delta t} \sim \prod_j e^{-ih_j P_j \Delta t}. \tag{17}$$

If operators A and B commute with each other, the first-order Trotter expansion becomes exact, i.e., $e^{A+B} = e^A e^B$. Therefore, a more insightful way to do Trotter expansion than the

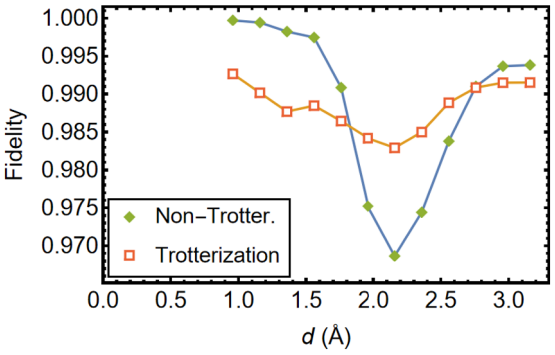

FIG. 13. The fidelity of the ground state of H_2O for the GeoQAE with exact discrete evolution operators (diamonds) and GeoQAE with Trotter expansions (squares). The H-O-H angle is fixed to the equilibrium angle, $\theta = 104.45^\circ$. We set $T = 10$ and $M = 20$ for both methods.

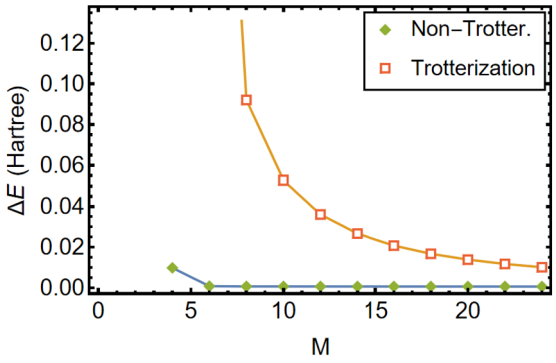

FIG. 14. The ground-state energy of H_2O at the O-H distance $d = 1.158$ Å with different discretization number M, obtained with the GeoQAE with exact evolution operators (diamonds) and GeoQAE with Trotter expansions (squares). $T = 10$ is used for both methods.

naive approach is to divide the Hamiltonian into subsets of commuting Hamiltonians [26],

$$H = \sum_j S_j, \tag{18}$$

$$S_j = \sum_k h_{jk} P_k, \tag{19}$$

where all P_k commute with each other within each S_j and $h_{jk} = 0$ if P_k does not belong to S_j. Thus, one can rewrite the original expansion as

$$e^{-iH\Delta t} \sim \prod_j e^{-iS_j\Delta t} = \prod_j \left(\prod_k e^{-ih_{jk}P_k\Delta t} \right). \tag{20}$$

Since the second step is exact, the error of this expansion only comes from the first step of decomposition. To further reduce the expansion errors, one can choose S_1 as the MC Hamiltonian of H, and S_2 as the MC Hamiltonian of $H \setminus S_1$, and repeating such procedure until only one term is left or the rest of the terms commute to each other. As finding the MC Hamiltonian is NP hard, one can use the greedy algorithm to get an approximate solution. In addition, for the evolution from $H^P_{\text{full}}(r_i)$ to $H^P_{\text{full}}(r_{i+1})$, the forms of Pauli operators do not change. Therefore, one can use a reference Hamiltonian, e.g., $1/2[H^P_{\text{full}}(r_i) + H^P_{\text{full}}(r_{i+1})]$, to determine the forms of S_j, and only change coefficients h_{jk} during each step of evolution.

We compare the results of the above Trotter expansion methods with those from the exact (but discretized) evolution operator from GeoQAE as used in Eq. (16). As shown in Figs. 12 and 13, the accuracy of the Trotter expansion is comparable with the exact evolution operator. The error of the Trotter expansion and exact evolution operators are 10^{-4} and 10^{-6} at $d = 0.958$ Å, and become even closer to each other when d gets larger. We also study the effect of discretization number M for H_2O molecule evolving from $H^P_I(r_1 = 0.958$ Å) to $H^P_{\text{full}}(r_1)$ and finally reaching $H^P_{\text{full}}(r_2 = 1.158$ Å), as shown in Fig. 14 and 15. We find that the Trotter expansion introduces large errors at small M, and when $M \gtrsim 20$, the

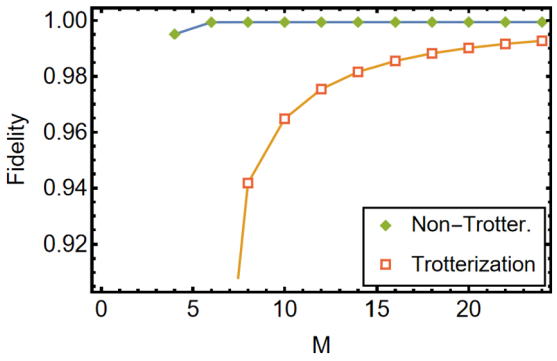

FIG. 15. The fidelity of the ground state of H_2O at the O-H distance $d = 1.158$ Å with different discretization number M, obtained with the GeoQAE with exact evolution operators (diamonds) and GeoQAE with Trotter expansions (squares). $T = 10$ is used for both methods.

energy (within ∼0.02 Hartree) and fidelity (within ∼0.01) obtained from the Trotter expansion is very close to the exact evolution operators.

C. Effects of noise and errors of real machine

To run GeoQAE on current digital quantum computers, one need perform the evolution operators hundreds of times. Due to the intrinsic noise of the physical systems in current quantum computers, such large number of gate operations may result in substantially inaccurate results. Here we use random bit-flipping errors as an example to demonstrate the substantial effects of noise on our GeoQAE method. We first use the Trotter expansion method described in Sec. VI B to construct a sequence of Pauli rotations, then with probability P randomly add an X gate on a randomly chosen qubit after each Pauli rotation. As shown in Fig. 16, even with very small probability of bit flipping, the energy results are far away from the exact one. This indicates that the GeoQAE method is currently not yet practical for noisy quantum machines. However, there was an experiment [27] that demonstrated a digitized

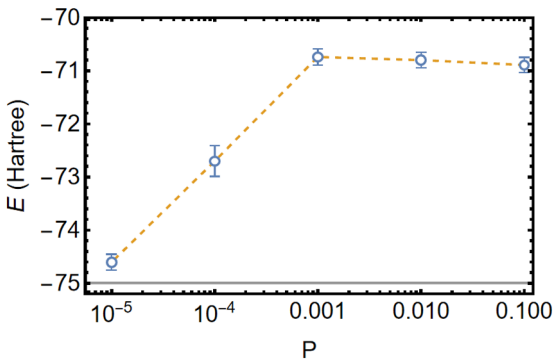

FIG. 16. The energy results of the ground state of H_2O at the O-H distance $d = 1.158$ Å with different flipping error probability P, obtained with the GeoQAE with Trotter expansions and a random flipping gate (X) on each qubit after each Trotter gate. $T = 10$, $M = 20$ is used for all the points. The gray line indicates the exact result $E = -74.998$ Hartree.

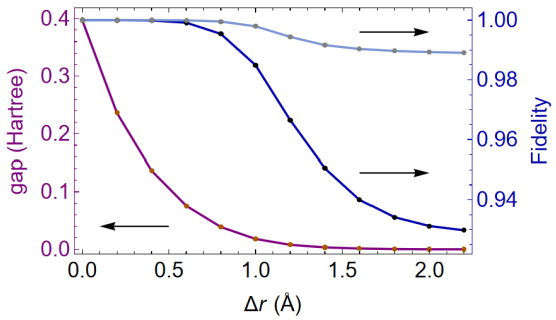

FIG. 17. The dependence of the energy gaps of one-step GeoQAE evolution and the fidelity of the ground-state wave functions of H_2O on the bond change Δr. The evolution is from $H^P_{\text{full}}(r_0)$ to $H^P_{\text{full}}(r_0 + \Delta r)$, with initial O-H bond length $r_0 = 0.958$ Å and H-O-H angle fixed $\theta = 104.45^\circ$. The gap minimum between the ground state and the first excited state for $H(s) = (1-s)H^P_{\text{full}}(r_0) + sH^P_{\text{full}}(r_0 + \Delta r)$ shows a trend of exponential decay with Δr. The upper fidelity curve is obtained with $T = 160$ and $M = 80$ and the lower fidelity curve is obtained with $T = 40$ and $M = 20$. There is a substantial improvement using larger T and M values.

adiabatic procedure for Ising systems with smaller number of qubits and Trotter steps; there one obtained good results. Thus, with the development of the scaling and accuracy of quantum computers, one can expect the GeoQAE method may become realizable in the future.

D. Effects of the discretization of the geometric path

The discretization of the geometric path is also an important factor of the GeoQAE algorithm. In this work, we vary bond slightly $\Delta r \equiv r_{i+1} - r_i$ in each step from r_i to r_{i+1}. While Δr needs to be small enough to ensure that the physical evolution is continuous, if it is too small, the computational time becomes too long and errors will accumulate rapidly. Therefore, Δr needs to chosen carefully. In essence, the robustness of the GeoQAE algorithm relies on the continuity of the Hamiltonians when atoms are displaced gradually along the geometric path (see Appendix D for several methods we use to ensure the continuity in the Hamiltonians). When Δr is sufficiently small, the one- and two-body coefficients in H_{full} are expected to vary slowly, which ensures the finite separation of energy levels in $H^{\text{Geo}}(s)$. In our calculations, we found $\Delta r \approx 0.1|\boldsymbol{r}_0|$ as a good empirical rule in the GeoQAE.

Here we investigate the effects of Δr on the energy gap and the fidelity of the H_2O system as an example. When Δr gets larger, it requires fewer accumulated steps to evolve to the desired bond length. However, within each evolution from one distance to another, the minimum gap will becomes smaller. Thus, we need longer evolution time for each step in order to achieve the same accuracy. As shown in Fig. 17, the energy gaps decrease exponentially with Δr as expected. However, at a moderate size $\Delta r = 1.0$ Å with small energy gaps (about 0.02 Hartree), the fidelity of the final ground state still remains high (above 0.98) with $T = 40$ and $M = 20$. Even with $\Delta r = 2.0$ Å, the ground-state fidelity can still reach a value of 0.93, which can be further improved to 0.99 with larger parameter values $T = 160$ and $M = 80$ (four times more discretization steps).

In this study, we only consider the geometric path defined by simple atomic distances. For more complicated cases, one can define the coordinate of collective variables and identify critical points that requires the GeoQAE to provide the accurate answer. For instance, the reaction coordinate is often used to study chemical reactions, connecting initial state, transition state, and final state on the potential energy surface. To obtain the ground-state energy of the transition state, a geometric path can be chosen along the reaction coordinate. For a given target geometry, there is vast degree of freedom to choose the geometric path. In principle, this degree of freedom can be explored to find optimal paths, where a sizable energy gap is maintained. This can be an interesting research topic, but it is beyond the scope of the current work.

VII. CONCLUSION

We have substantially improved an adiabatic algorithm for computing the ground state and low-lying excited states of molecules (MC-QAE) proposed in a previous work by introducing a geometric adiabatic evolution path (GeoQAE). The idea of choosing a suitable Hamiltonian that can be connected naturally and smoothly to the final Hamiltonian can be applied to other many-body problems. In our present focus on the molecular energy, the MC Hamiltonian associated with a particular final molecular Hamiltonian generalizes the Fock operator such that the Hartree-Fock ground state is an eigenstate with the eigenenergy being the Hartree-Fock ground-state energy.

We showed by numerical simulations of the adiabatic evolution that the GeoQAE approach gives significant improvement on both ground-state energies and the fidelity of wave functions (as well as few lowest excited states) for different molecules in the region where the MC-QAE fails due to energy level crossing. We also demonstrated its potential application by simulating the potential energy surface for an exemplary chemical reaction involving two pairs of molecules.

Although on the present noisy quantum devices, the GeoQAE approach might not yet be implemented to yield accurate results due to the required large gate numbers for the evolution operators, hardware is continuing to be improved and this may make our algorithm practical in the future. Moreover, the existence of gaps in the suitably chosen geometric path may allow alternative quantum approximate optimization algorithm (QAOA)-like approaches or better variational *Ansätze* to be developed.

ACKNOWLEDGMENTS

Part of this work (in particular the research on the connection of the maximally commuting Hamiltonian to the Hartree-Fock solution) was supported by the National Science Foundation under Grant No. PHY 1915165 (T.-C.W.). The part of the research that involves quantum chemistry applications used the theory and computation resources of the Center for Functional Nanomaterials (CFN), which is a U.S. Department of Energy Office of Science User Facility, at the Brookhaven National Laboratory under Contract No. DE-SC0012704 by the U.S. Department of Energy, Office of Science (D.L. and Q.W.). The research on the quantum algorithmic development in this work was supported by the U.S. Department of Energy, Office of Science, National Quantum Information Science Research Centers, Co-design Center for Quantum Advantage (C2QA) under Contract No. DE-SC0012704 (H.Y and T.-C.W.).

APPENDIX A: MAPPING FERMIONIC OPERATORS TO QUBITS

Here we briefly review two widely used methods to map the fermionic operators to Pauli operators.

1. Jordan-Wigner mapping

The Jordan-Wigner transformation is a widely used method for mapping fermions (a's) to spins (σ's),

$$a_k = \left(\prod_{j=1}^{k} \sigma_j^z\right)\left(\sigma_k^x + i\sigma_k^y\right)/2, \tag{A1}$$

$$a_k^\dagger = \left(\prod_{j=1}^{k} \sigma_j^z\right)\left(\sigma_k^x - i\sigma_k^y\right)/2. \tag{A2}$$

Let the spin state $|-1\rangle$ be qubit state $|1\rangle_q$ and $|+1\rangle$ be $|0\rangle_q$, it can be easily verified that the fermionic state $|0\rangle_f$ will be transformed to $|0\rangle_q$ and $|1\rangle_f$ to $|1\rangle_q$. Thus, the mapping keeps the wave function in the same expression. For example, the wave function in the fermionic basis $|1011\rangle_f$ will be mapped to qubit vector $|1011\rangle_q$.

2. Parity mapping and qubit reduction

Parity mapping is a method to map the wave function from the fermion-occupation basis to the so-called parity basis. Let f_j (can only be 0 or 1 for fermions) be the occupation number in the fermionic basis, and $p_j = (\sum_{i=1}^{j} f_j \mod 2)$ counts the parity of the orbitals up to j, the parity basis can be chosen as $|p_1 p_2 \dots p_n\rangle$. And the corresponding transformation is [17]

$$a_k = \frac{1}{2}\left(\prod_{j=k+1}^{n} \sigma_j^x\right)\left(\sigma_k^x \sigma_{k-1}^z + i\sigma_k^y\right), \tag{A3}$$

$$a_k^\dagger = \frac{1}{2}\left(\prod_{j=k+1}^{n} \sigma_j^x\right)\left(\sigma_k^x \sigma_{k-1}^z - i\sigma_k^y\right). \tag{A4}$$

Our label for fermions and qubits begin at 1 and we define the operator σ_0^z to be the identity matrix. One can verify that the fermionic basis $|f_1 \dots f_n\rangle$ can be mapped to the parity basis $|p_1 \dots p_n\rangle$ according to the definition of p_is. For example, the fermionic state $|101110\rangle_f$ will be mapped to parity state $|110100\rangle_p$.

Now consider a fermionic state with spin configuration $|f_1^\alpha \dots f_n^\alpha, f_{n+1}^\beta \dots f_{2n}^\beta\rangle$ and its parity correspondence $|p_1 \dots p_n, p_{n+1} \dots p_{2n}\rangle$. Note that the p_n counts for the parity of all α-spin orbitals and p_{2n} counts for the parity of all orbitals. Therefore, if one further assumes the conservation of the spin and particle number, the parity numbers p_n, p_{2n} are constants. Thus, one can remove the two qubits and only consider the subspace spanned by states with same electron

number and spin configuration, which reduces the complexity of both quantum computations and classical simulations.

APPENDIX B: BRIEF REVIEW OF THE HARTREE-FOCK METHOD

Here we summarize the Hartree-Fock procedure so as to introduce the notation used in the main text of the paper. We refer the readers to standard textbooks such as Ref. [1], for more details. Given a molecule, our goal is to solve the time-independent electronic Schrödinger equation,

$$\left[-\frac{1}{2}\sum_i \nabla_i^2 - \frac{1}{2}\sum_I \frac{\nabla_I^2}{M_I/m_e} - \sum_{A,i}\frac{Z_A}{r_{Ai}} + \sum_{A>B}\frac{Z_A Z_B}{R_{AB}} + \sum_{i>j}\frac{1}{r_{ij}}\right]\tilde{\Psi}(\mathbf{r};\mathbf{R}) = E\tilde{\Psi}(\mathbf{r};\mathbf{R}), \tag{B1}$$

where $\tilde{\Psi}$ is the wave function for both nuclei and electrons, Z_I is the atomic number for atom I (whose nucleus shares the same symbol and has mass M_I), i and j index electrons (whose mass is denoted by m_e, and charge e is set to unity). If we are only interested in the electronic wave functions, we can treat the nuclei as fixed point charges, and the Hamiltonian will be simplified to

$$\left[-\frac{1}{2}\sum_i \nabla_i^2 - \sum_{A,i}\frac{Z_A}{r_{Ai}} + \sum_{i>j}\frac{1}{r_{ij}}\right]\Psi(\mathbf{r};\mathbf{R}) = E_{el}\Psi(\mathbf{r};\mathbf{R}), \tag{B2}$$

where $\Psi(\mathbf{r};\mathbf{R})$ now represents the electronic wave function, with nuclei positions $\mathbf{R}$ as parameters. Suppose we use single Slater determinants as one-electron wave function, and introduce fermionic creation operators and annihilation operators, the Hamiltonian can be written in the second quantized picture

$$H_{el} = \sum_{i,j} t_{ij} a_i^\dagger a_j + \frac{1}{2}\sum_{i,j,k,l} u_{ijkl} a_i^\dagger a_k^\dagger a_l a_j, \tag{B3}$$

where

$$t_{ij} = \langle i|h|j\rangle = \int d\mathbf{x}_1 \chi_i^*(\mathbf{x}_1)\left(-\frac{1}{2}\nabla_1^2 - \sum_A \frac{Z_A}{r_{A1}}\right)\chi_j(\mathbf{x}_1) \tag{B4}$$

and

$$u_{ijkl} = [ij \mid kl] = \int d\mathbf{x}_1 d\mathbf{x}_2 \chi_i^*(\mathbf{x}_1)\chi_j(\mathbf{x}_1)\frac{1}{r_{12}}\chi_k^*(\mathbf{x}_2)\chi_l(\mathbf{x}_2) \tag{B5}$$

were introduced in the main text. The energy expression becomes

$$E_{el} = \langle\Psi|\hat{H}_{el}|\Psi\rangle = \sum_i \langle i|h|i\rangle + \frac{1}{2}\sum_{ij}([ii \mid jj] - [ij \mid ji]). \tag{B6}$$

In Hartree-Fock method, we assume the ground-state wave function can be approximated by a single Slater determinant, and the Hamiltonian can be reduced to a one-body Hamiltonian,

$$\hat{f} = \sum_{i,j}(t_{ij} + V_{ij})a_i^\dagger a_j, \tag{B7}$$

$$V_{ij} = \sum_{k\in\text{occ}}(u_{ikkj} - u_{ikjk}), \tag{B8}$$

where $\hat{f}$ is referred to as the Fock operator. In the Hartree-Fock calculation, we seek for an optimal molecular basis set (labeled by Greek letters in the main text) that can minimize the energy expectation value, starting from a chosen set of atomic orbitals (labeled by Roman letters), such as the STO-3G basis set. An iterative calculation can be performed to obtain the optimal molecular basis set. After we obtain one basis set for the Fock operator, we diagonalize the operator and rewrite the full Hamiltonian in the new basis set, then perform the diagonalization again until the result converges. We use the quantum chemistry package PYSCF [21] to perform this classical step of calculations.

APPENDIX C: JORDAN-WIGNER MAPPING OF THE INITIAL HAMILTONIAN AND ITS RELATION TO THE HARTREE-FOCK SOLUTION

Here we use Jordan-Wigner mapping as an example to show the connection between our choice of the initial Hamiltonian and the classical Hartree-Fock method. Suppose after a classical Hartree-Fock calculation, we get a set of converged orbital basis $\{|\psi_\alpha\rangle\}$ and their corresponding creation and annihilation operators a_α, $a_\alpha^\dagger$, the full Hamiltonian in the second quantization picture is

$$H_{\text{full}}^F = \sum_{\alpha,\beta} t_{\alpha\beta}^{\text{MO}} a_\alpha^\dagger a_\beta + \frac{1}{2}\sum_{\alpha,\beta,\gamma,\delta} u_{\alpha\beta\gamma\delta}^{\text{MO}} a_\alpha^\dagger a_\gamma^\dagger a_\delta a_\beta,$$

which, by Jordan-Wigner mapping, results in a summation of Pauli operators $H_P = \sum P_i$. And our choice of the initial Hamiltonian for the Pauli operators is the summation only over the terms containing only Zs and Is, which originate from the terms of the fermionic operators that only contains number operators $a^\dagger a$,

$$H_I^F = \sum_\alpha t_{\alpha\alpha}^{\text{MO}} a_\alpha^\dagger a_\alpha + \frac{1}{2}\sum_{\alpha,\beta}\left(u_{\alpha\alpha\beta\beta}^{\text{MO}} a_\alpha^\dagger a_\beta^\dagger a_\beta a_\alpha - u_{\alpha\beta\beta\alpha}^{\text{MO}} a_\alpha^\dagger a_\beta^\dagger a_\alpha a_\beta\right). \tag{C1}$$

Note that due to the choice of our molecular basis, the $|\psi_\alpha\rangle$s are converged Hartree-Fock molecular basis. Thus, the Hartree-Fock state in the fermionic basis is simply occupying the lowest-energy orbitals. Suppose the wave function for orbital labels $f_1^\alpha, f_2^\alpha, \ldots$ with lowest energy first (for same spins) and consisting of α and β spin takes the form $|f_1^\alpha \ldots f_n^\alpha, f_{n+1}^\beta \ldots f_{2n}^\beta\rangle$, the Hartree-Fock wave function for a four-electron and eight-orbital state is $|1100, 1100\rangle$. It is obvious that the state is one of the eigenstates of our initial Hamiltonian Eq. (C1), with corresponding

eigenenergy

$$H_I^F\,|\psi_{\rm HF}\rangle = \left(\sum_{\alpha\in{\rm occ}} t^{\rm MO}_{\alpha\alpha} + \frac{1}{2}\sum_{\alpha,\beta\in{\rm occ}}\left(u^{\rm MO}_{\alpha\alpha\beta\beta} - u^{\rm MO}_{\alpha\beta\beta\alpha}\right)\right)|\psi_{\rm HF}\rangle\,. \tag{C2}$$

Comparing the value with the expression of the Hartree-Fock energy Eq. (8), one can verify that they are exactly the same. Therefore, the Hartree-Fock wave function is an eigenstate of our initial Hamiltonian with the eigenenergy equal to the Hartree-Fock energy. We remark that the Hartree-Fock state is not always the ground state of the H_I^F (while in most cases where the bond lengths are near equilibrium, it is), and the fermionic Hamiltonian H_I^F is also different from the conventional definition of Hartree-Fock Hamiltonian Eq. (B7), where only one-body terms are contained.

APPENDIX D: METHODS TO ENSURE THE CONTINUITY OF THE HAMILTONIAN

The energy gap for the evolution from $H^P_{\rm full}(\boldsymbol{r})$ to $H^P_{\rm full}(\boldsymbol{r}+\Delta\boldsymbol{r})$ rely on the continuity of the Hamiltonian with respect to geometric configuration $\boldsymbol{r}$. If the Hamiltonian difference $|H^P_{\rm full}(\boldsymbol{r}) - H^P_{\rm full}(\boldsymbol{r}+\Delta\boldsymbol{r})|$ is small, then the changes of the spectrum are also small, which gives rise to a relatively large energy gap during the evolution so that the evolving state is not likely to mix with other energy levels; see, e.g., Fig. 1(b). Since the $H^P_{\rm full}(\boldsymbol{r})$ is transformed from the fermionic Hamiltonian $H^F_{\rm full}(\boldsymbol{r})$, the continuity of $H^P_{\rm full}(\boldsymbol{r})$ is equivalent to that of $H^F_{\rm full}(\boldsymbol{r})$, which is essentially the continuity of $t^{\rm MO}_{\alpha\beta}(\boldsymbol{r})$ and $u^{\rm MO}_{\alpha\beta\gamma\delta}(\boldsymbol{r})$. If we choose a fixed basis for all configurations of a molecule, the continuity is guaranteed by the physical continuity of the Hamiltonian with respect to the geometric configuration $\boldsymbol{r}$. However, our choice for each configuration is the Hartree-Fock molecular basis, which depends on the Hartree-Fock calculation at each geometric configuration and is not necessarily continuous with bond length. We will discuss below several methods to ensure the continuity of the $H^P_{\rm full}(\boldsymbol{r})$. We emphasize again that for our purpose it is not important how good the Hartree-Fock solution is to the exact solution but continuity of the Hamiltonians $H^P_{\rm full}(\boldsymbol{r})$ as $\boldsymbol{r}$ varies.

1. Initial guess

The efficiency and convergence of a Hartree-Fock calculation depends largely on the choice of the initial guess. In our algorithm, we need the Hartree-Fock molecular bases for a series geometric configurations $\boldsymbol{r}_0, \boldsymbol{r}_1, \ldots, \boldsymbol{r}_N$, where $\boldsymbol{r}_0$ is chosen to be a near-equilibrium configuration and the distances between each successive configurations $|\boldsymbol{r}_{n+1} - \boldsymbol{r}_n|$ are small. Since the difference of the two configurations is small, the Hartree-Fock calculation results of them are close to each other. Thus, the converged basis from previous configuration is a good initial guess for the next configuration and a Hartree-Fock calculation is likely to converge near the initial basis.

Therefore, for a given configuration $\boldsymbol{r}_n$ of the molecule, our choice of initial guess is chosen to be the converged density matrix at previous configuration $\boldsymbol{r}_{n-1}$. For the initial configuration $\boldsymbol{r}_0$, we can choose any initial guess that gives a converged result.

2. Permutations and signs of the molecular basis

Suppose we have obtained a set Hartree-Fock molecular basis states $\{|\varphi_i\rangle_{\boldsymbol{r}}\}$ at configuration $\boldsymbol{r}$, it is obvious that, if we perform a permutation $|\varphi_1'\rangle = |\varphi_2\rangle\,,\ |\varphi_2'\rangle = |\varphi_1\rangle$, or add a minus sign $|\varphi_1'\rangle = -|\varphi_1\rangle$, the new molecular basis set is equivalent as before. However, after one does such transformation to the basis, the Hamiltonian should also be transformed accordingly. And such transformation will result in a noticeable nonvanishing increase of the difference of the Hamiltonians $|H^P_{\rm full}(\boldsymbol{r}) - H^P_{\rm full}(\boldsymbol{r}+\Delta r)|$ (compared to the case where the bases at both distances are very similar, even in terms of their ordering) despite that $\Delta\boldsymbol{r}$ is very close to 0.

To solve this problem, we manually perform a proper permutation and a suitable sign change (if necessary) to realign and enforce the molecular basis $\{|\varphi_i\rangle_{\boldsymbol{r}+\Delta\boldsymbol{r}}\}$ at $\boldsymbol{r}+\Delta r$ consistent with $\{|\varphi_i\rangle_{\boldsymbol{r}}\}$ at $\boldsymbol{r}$, so that the basis is continuous with respect to the change in the geometric configuration $\boldsymbol{r}$. In our calculation, the molecular orbitals $|\varphi_i\rangle$ are written in combinations of atomic orbitals $|\varphi_i\rangle = \sum_j C_{ij}\,|\phi_j^{\rm AO}\rangle$, where the superscript AO denotes the atomic orbitals, which are constructed locally and automatically continuous with geometric configuration $\boldsymbol{r}$. Therefore, by comparing and realigning the molecular coefficients $C_{ij}^{(\boldsymbol{r})}$ and $C_{ij}^{(\boldsymbol{r}+\Delta\boldsymbol{r})}$ at the successive configurations $\boldsymbol{r}$, $\boldsymbol{r}+\Delta\boldsymbol{r}$, one can ensure the continuity of the Hartree-Fock molecular basis with respect to the geometric configuration $\boldsymbol{r}$.

3. Transforming the unconverged molecular basis

In some cases where the Hartree-Fock calculation is hard to converge and cannot be improved by choosing a good initial guess, we need to abandon the quality of the Hartree-Fock results to ensure the continuity of the Hamiltonian $H^P_{\rm full}(\boldsymbol{r})$. To do this, we use the molecular coefficients $C_{ij}^{(\boldsymbol{r}_n)}$ at the previous configuration $\boldsymbol{r}_n$ to calculate the molecular basis at next configuration $\boldsymbol{r}_{n+1}$

$$|\varphi_i\rangle_{\boldsymbol{r}_{n+1}} \simeq \sum_j C_{ij}^{(\boldsymbol{r}_n)}\,\left|\phi_j^{\rm AO}\right\rangle_{\boldsymbol{r}_{n+1}}. \tag{D1}$$

Note that the atomic orbitals are not necessarily orthogonal to each other. We need additional transformations to ensure $|\varphi_i\rangle_{\boldsymbol{r}_{n+1}}$ is an orthonormal basis. Denote $S_{ij}^{(\boldsymbol{r}_n)} = \langle\phi_i^{\rm AO}|\phi_j^{\rm AO}\rangle_{\boldsymbol{r}_n}$ and $S_{ij}^{(\boldsymbol{r}_{n+1})} = \langle\phi_i^{\rm AO}|\phi_j^{\rm AO}\rangle_{\boldsymbol{r}_{n+1}}$, and assume the molecular basis at $\boldsymbol{r}_n$ is already orthonormal $\langle\varphi_i|\varphi_j\rangle_{\boldsymbol{r}_n} = \delta_{ij}$. We construct the molecular basis at $\boldsymbol{r}_{n+1}$:

$$\begin{aligned}|\varphi_i\rangle_{\boldsymbol{r}_{n+1}} &= \sum_{j,k,l} C_{ij}^{(\boldsymbol{r}_n)}(S^{(\boldsymbol{r}_n)})^{\frac{1}{2}}_{jk}(S^{(\boldsymbol{r}_{n+1})})^{-\frac{1}{2}}_{kl}\,\left|\phi_l^{\rm AO}\right\rangle_{\boldsymbol{r}_{n+1}}\\ &\equiv \sum_l D_{il}^{(\boldsymbol{r}_{n+1})}\,\left|\phi_l^{\rm AO}\right\rangle_{\boldsymbol{r}_{n+1}},\end{aligned} \tag{D2}$$

where the matrix power operation $A^{1/2}$ is defined as follows: if matrix A can be diagonalized $A = U^T\Lambda U$ and Λ is a positive diagonal matrix, we define $A^{1/2} = U^T\Lambda^{1/2}U$. One can easily verify that $\langle\varphi_i|\varphi_j\rangle_{\boldsymbol{r}_{n+1}} = \delta_{ij}$. Note that matrix $S^{(\boldsymbol{r})}$ is only related to $|\phi^{\rm AO}\rangle_{\boldsymbol{r}}$. If $\Delta\boldsymbol{r} = \boldsymbol{r}_{n+1} - \boldsymbol{r}_n$ is small enough, we have

$|\phi_l^{\mathrm{AO}}\rangle_{\boldsymbol{r}_{n+1}} \sim |\phi_l^{\mathrm{AO}}\rangle_{\boldsymbol{r}_n}$ and $S^{(\boldsymbol{r}_n)} \sim S^{(\boldsymbol{r}_{n+1})}$. Thus,

$$|\varphi_i\rangle_{\boldsymbol{r}_{n+1}} \sim \sum_j C_{ij}^{(\boldsymbol{r}_n)} |\phi_l^{\mathrm{AO}}\rangle_{\boldsymbol{r}_n} = |\varphi_i\rangle_{\boldsymbol{r}_n} . \tag{D3}$$

After transforming the Hamiltonian $H_{\mathrm{full}}^P(\boldsymbol{r}_{n+1})$ according to the new molecular basis Eq. (D2), we assure the continuity of the Hamiltonian.

[1] A. Szabo and N. S. Ostlund, *Modern Quantum Chemistry: Introduction to Advanced Electronic Structure Theory* (Courier Corporation, Chelmsford, 2012).

[2] S. McArdle, S. Endo, A. Aspuru-Guzik, S. C. Benjamin, and X. Yuan, Quantum computational chemistry, Rev. Mod. Phys. **92**, 015003 (2020).

[3] A. Aspuru-Guzik, A. D. Dutoi, P. J. Love, and M. Head-Gordon, Simulated quantum computation of molecular energies, Science **309**, 1704 (2005).

[4] A. Peruzzo, J. McClean, P. Shadbolt, M.-H. Yung, X.-Q. Zhou, P. J. Love, A. Aspuru-Guzik, and J. L. O'Brien, A variational eigenvalue solver on a photonic quantum processor, Nature Commun. **5**, 4213 (2014).

[5] A. Kandala, A. Mezzacapo, K. Temme, M. Takita, M. Brink, J. M. Chow, and J. M. Gambetta, Hardware-efficient variational quantum eigensolver for small molecules and quantum magnets, Nature (London) **549**, 242 (2017).

[6] J. Du, N. Xu, X. Peng, P. Wang, S. Wu, and D. Lu, NMR Implementation of a Molecular Hydrogen Quantum Simulation with Adiabatic State Preparation, Phys. Rev. Lett. **104**, 030502 (2010).

[7] R. Babbush, P. J. Love, and A. Aspuru-Guzik, Adiabatic quantum simulation of quantum chemistry, Sci. Rep. **4**, 6603 (2015).

[8] R. Xia, T. Bian, and S. Kais, Electronic structure calculations and the ising hamiltonian, J. Phys. Chem. B **122**, 3384 (2018).

[9] M. Streif, F. Neukart, and M. Leib, Solving quantum chemistry problems with a *d*-wave quantum annealer, in *International Workshop on Quantum Technology and Optimization Problems* (Springer, Berlin, 2019), pp. 111–122.

[10] B. P. Lanyon, J. D. Whitfield, G. G. Gillett, M. E. Goggin, M. P. Almeida, I. Kassal, J. D. Biamonte, M. Mohseni, B. J. Powell, M. Barbieri *et al.*, Towards quantum chemistry on a quantum computer, Nature Chem. **2**, 106 (2010).

[11] J. I. Colless, V. V. Ramasesh, D. Dahlen, M. S. Blok, M. E. Kimchi-Schwartz, J. R. McClean, J. Carter, W. A. De Jong, and I. Siddiqi, Computation of Molecular Spectra on a Quantum Processor with an Error-Resilient Algorithm, Phys. Rev. X **8**, 011021 (2018).

[12] A. Kandala, K. Temme, A. D. Córcoles, A. Mezzacapo, J. M. Chow, and J. M. Gambetta, Error mitigation extends the computational reach of a noisy quantum processor, Nature (London) **567**, 491 (2019).

[13] P. J. Ollitrault, A. Kandala, C.-F. Chen, P. K. Barkoutsos, A. Mezzacapo, M. Pistoia, S. Sheldon, S. Woerner, J. M. Gambetta, and I. Tavernelli, Quantum equation of motion for computing molecular excitation energies on a noisy quantum processor, Phys. Rev. Research **2**, 043140 (2020).

[14] H. R. Grimsley, S. E. Economou, E. Barnes, and N. J. Mayhall, An adaptive variational algorithm for exact molecular simulations on a quantum computer, Nature Commun. **10**, 3007 (2019).

[15] H. Yu and T.-C. Wei, Quantum zeno approach for molecular energies with maximum commuting initial hamiltonians, Phys. Rev. Research **3**, 013104 (2021).

[16] I. N. Levine, D. H. Busch, and H. Shull, *Quantum Chemistry* (Pearson Prentice Hall, Upper Saddle River, 2009), Vol. 6.

[17] J. T. Seeley, M. J. Richard, and P. J. Love, The Bravyi-Kitaev transformation for quantum computation of electronic structure, J. Chem. Phys. **137**, 224109 (2012).

[18] K. Setia and J. D. Whitfield, Bravyi-Kitaev superfast simulation of electronic structure on a quantum computer, J. Chem. Phys. **148**, 164104 (2018).

[19] K. Setia, S. Bravyi, A. Mezzacapo, and J. D. Whitfield, Superfast encodings for fermionic quantum simulation, Phys. Rev. Research **1**, 033033 (2019).

[20] M. A. Nielsen and I. Chuang, *Quantum Computation and Quantum Information* (Cambridge University Press, Cambridge, 2002).

[21] Q. Sun, T. C. Berkelbach, N. S. Blunt, G. H. Booth, S. Guo, Z. Li, J. Liu, J. D. McClain, E. R. Sayfutyarova, S. Sharma, S. Wouters, and G. K.-L. Chan, PySCF: the Python-based simulations of chemistry framework, WIREs Comput. Mol. Sci. **8**, e1340 (2018).

[22] H. Abraham *et al.*, Qiskit: An open-source framework for quantum computing (2019), doi: 10.5281/zenodo.2573505.

[23] C. Yi and E. Crosson, Spectral analysis of product formulas for quantum simulation, npj Quantum Inf. **8**, 37 (2022).

[24] N. Balakrishnan, Perspective: Ultracold molecules and the dawn of cold controlled chemistry, J. Chem. Phys. **145**, 150901 (2016).

[25] K. Gasperich, M. Deible, and K. D. Jordan, H4: A model system for assessing the performance of diffusion monte carlo calculations using a single slater determinant trial function, J. Chem. Phys. **147**, 074106 (2017).

[26] P. Gokhale, O. Angiuli, Y. Ding, K. Gui, T. Tomesh, M. Suchara, M. Martonosi, and F. T. Chong, Minimizing state preparations in variational quantum eigensolver by partitioning into commuting families, arXiv:1907.13623 (2019).

[27] R. Barends, A. Shabani, L. Lamata, J. Kelly, A. Mezzacapo, U. Las Heras, R. Babbush, A. G. Fowler, B. Campbell, Y. Chen *et al.*, Digitized adiabatic quantum computing with a superconducting circuit, Nature (London) **534**, 222 (2016).